Low emittance electron beam formation with a 17 GHz RF gun

W. J. Brown, S. E. Korbly, K. E. Kreischer, I. Mastovsky, and R. J. Temkin
MIT, Plasma Science and Fusion Center, 167 Albany Street, Cambridge, Massachusetts 02139
(Received 30 January 2001; published 20 August 2001)

We report on electron beam quality measurement results from the Massachusetts Institute of Technology 17 GHz RF gun experiment. The 1.5 cell RF gun uses a solenoid for emittance compensation. It has produced bunch charges up to 0.1 nC with beam energies up to 1 MeV. The normalized rms emittance of the beam after 35 cm of transport from the gun has been measured by a slit technique to be 3π mm mrad for a 50 pC bunch. This agrees well with PARMELA simulations at these beam energies. At the exit of the electron gun, we estimate the emittance to be about 1π mm mrad, which corresponds to a beam brightness of about 80 $A/(\pi \text{ mm mrad})^2$. Improved beam quality should be possible with a higher energy output electron beam from the gun.

DOI: 10.1103/PhysRevSTAB.4.083501 PACS numbers: 29.25.Bx, 41.75.Fr, 41.75.Lx, 29.27.–a

I. INTRODUCTION

The Massachusetts Institute of Technology (MIT) 17 GHz photocathode RF gun is a 1.5 cell electron accelerating structure consisting of two coupled TM_{010} mode cavities excited by sidewall coupled microwaves from a WR-62 waveguide (Fig. 1). The goal of the MIT experiment is to examine the advantages of operating an electron source at high frequency, and thereby produce an ultrahigh quality electron beam capable of meeting the demands of future applications such as injectors for linear colliders or accelerators for short wavelength free electron lasers [1], the stringent requirements of which (100 A peak current, and 1π mm mrad rms normalized emittance) have been unrealized by conventional electron sources. The scaling with RF frequency of the quality of the beam from an RF gun was previously derived [2,3]. This study suggests that the emittance of the beam will scale inversely with RF frequency provided the charge and size of the beam are also scaled inversely with RF frequency (constant peak current) and the accelerating gradient is increased proportional to frequency. This implies that a quadratic increase in the beam brightness with RF frequency can, in principle, be obtained.

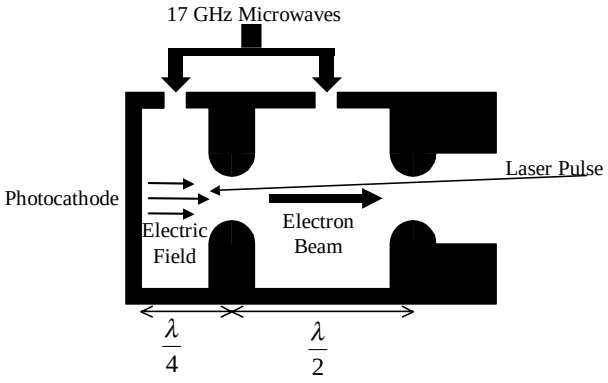

FIG. 1. Schematic of the RF Gun.

These favorable scaling laws coupled with the need for higher brightness beams have fueled an increasing interest in recent years in the use of high frequency RF guns, ranging from 8 GHz [4] to 17 GHz [5] and all the way up to 91 GHz [6]. However, the amount of experimental data from RF gun experiments operating above the SLAC frequency of 2.856 GHz has remained limited, making it difficult to verify that the ideal scaling laws, which rely on a number of assumptions such as proportionally higher accelerating gradients and emittance compensating magnetic fields, subpicosecond RF to laser timing stability, and tighter machine tolerances on manufactured parts, can be achieved in practice. Potential problems may also arise from the scaling of the electron bunch size with RF wavelength. Since the laser intensity must increase as the square of the RF frequency, optical breakdown on the photocathode surface will ultimately limit the degree to which the initial bunch size can be minimized while maintaining the $1/\omega$ charge scaling. In light of these challenges, the results obtained from the MIT 17 GHz RF gun provide valuable insight into the practical advantages of high frequency electron sources.

In this paper, we report on the successful high power operation of a 17 GHz RF gun, including the production of a high current (50 A peak), low emittance (3π mm mrad) beam, and the demonstration of good laser to RF phase stability with stable operation of the gun. We believe this demonstrates that the 17 GHz gun can be used to produce a high quality electron beam capable of meeting the demands of many future applications, including short wavelength free electron lasers and other coherent radiation sources.

II. GUN DESIGN AND THEORY

Initial experiments demonstrating beam production from a previous version of the 17 GHz RF gun were completed at MIT and were reported [7]. The results of beam measurements are listed in Table I. This was the first RF gun experiment to operate above 3 GHz.

TABLE I. Beam measurement results from the original experiment.

Parameter	Measurement
Bunch charge	0.1 nC
Initial bunch length	1 ps (laser measurement)
Initial bunch radius	0.5 mm (laser)
Peak cathode field	200 MV/m
Beam energy	1.05 MeV
Energy spread	2.5%

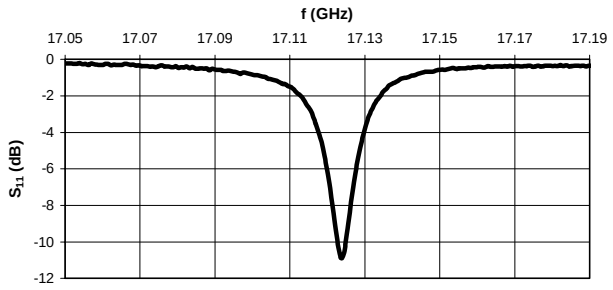

FIG. 2. Cold test of the new RF gun.

The results presented in this paper are for a new RF gun experiment. This experiment has a number of improvements over the previous experiment [7], including an improved beam line that features the addition of an emittance compensating solenoid and emittance diagnostics, as well as a new RF gun with improved longitudinal field balance. Field profile measurements of the original gun revealed the field strength in the half cell to be about 20% stronger than that in the full cell. To optimize the acceleration efficiency and maximize the accelerating gradient, the new gun was equipped with tuners in both cells to allow for field balance optimization. The tuners consist of small plungers which retract from or fill up a small hole in both the half cells and the full cells, but fall short of actually protruding into the cavity. This provides about 10 MHz of tunability without introducing protrusions into the cavity which could cause breakdown. To minimize the field asymmetries due to the coupling holes, it was ensured that the coupling factor would be less than or equal to unity (i.e., the coupling holes would not be larger than necessary). The measured S_{11} curve from a cold test of this structure is shown in Fig. 2. It can be determined from the S_{11} curve that the coupling coefficient of the gun is given by $\beta = 0.56$ and the Ohmic quality factor is $Q = 1700$.

Field profile measurements

A "bead hang" method was developed to perform field profile measurements of the excited mode in the MIT RF gun. This is similar to "bead pull" measurements [8] but, rather than being pulled all the way through the RF cavity, the perturbing element simply hangs down into it. The advantage of this method is that there is no need to have a hole in the cathode, allowing for the exact structure used in high power experiments to be measured. Ideally, the axial electric field profile $E(z)$ in the gun can then be determined by mapping the perturbation in the resonant frequency, $\Delta f(z)$, of the excited mode as a function of the position of the bead, i.e.,

$$|E(z)|^2 \propto \frac{\Delta f(z)}{\alpha_{\text{bead}}}, \tag{1}$$

where α_{bead} is the electric polarizability of the bead.

In reality, the line used to hang the bead into the cavity also has a position dependent effect on the resonant frequency. This nonlocal perturbation, which can be expressed as

$$\Delta f_{\text{line}}(z) \propto \int^{z} |E(\xi)|^2 \, d\xi \tag{2}$$

where the integral is along the length of the support line up to the position of the bead, should be subtracted out of the measurement in order to obtain accurate results. This is especially necessary for smaller, high frequency structures such as the MIT 17 GHz RF gun in which the line will have a more significant effect. The measured value for the electric field profile is then given by

$$|E(z)|^2 \propto \frac{[\Delta f(z) - \Delta f_{\text{line}}(z)]}{\alpha_{\text{bead}}}, \tag{3}$$

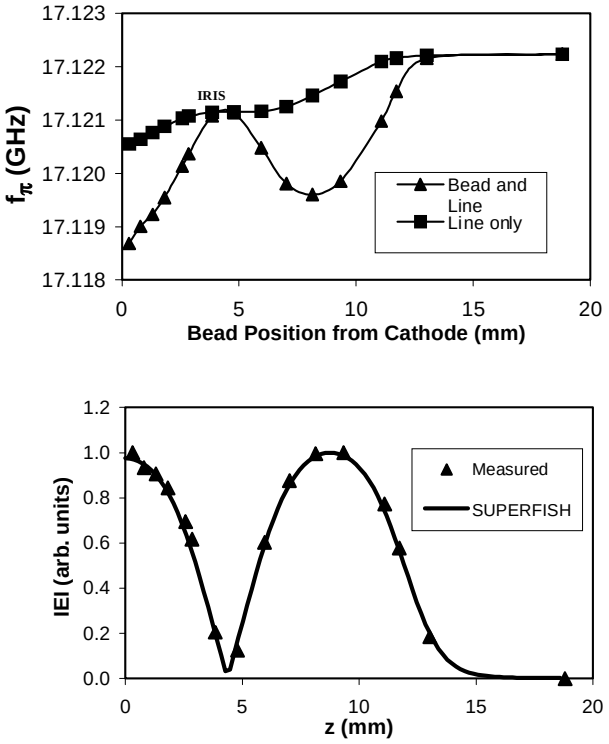

FIG. 3. Measurement of the on-axis field profile of the new RF gun. Top: Frequency perturbation as a function of bead position. Bottom: On-axis field profile derived from both measurement and SUPERFISH simulation.

where $\Delta f(z)$ is now the total frequency perturbation caused by the bead and the support line when the bead is at a position z from the cathode.

The results of a bead hang measurement of the new cavity are shown in Fig. 3. The bead used in the measurement was a 0.5 mm long, 0.2 mm diameter piece of copper wire. The support line used in the measurement was a short piece of 76 μm diameter plastic wire (fishing line rated at 0.7 kg tensile strength). As expected, the frequency perturbation due to the bead was zero at the position of the iris between the half cell and the full cell.

III. BEAM LINE DESIGN

A schematic of the beam line for the RF gun experiment is shown in Fig. 4. The UV drive laser is injected at near normal incidence by an aluminum mirror inside the laser injection chamber. The mirror is slightly offset from the beam axis to allow the electron beam to be transported to downstream diagnostics. Emittance compensation is performed with a 6.5 cm long, 5 kG peak field solenoid. The magnet consists of four double pancakes of 5×5 mm hollow core conductor, consisting of 80 total turns. In order to maximize the field inside the magnet and minimize it outside the magnet (i.e., at the cathode), the solenoid was encased in an iron yoke with an inside bore diameter of only 1.9 cm. The edge of the magnet is placed 2.0 cm from the gun cathode, resulting in a maximum magnetic field at the cathode of about 25 G. The additional normalized emittance resulting from this magnetic field is only 0.04π mm mrad for a 0.5 mm radius beam. The emittance is measured by breaking the beam into individual beamlets using an array of 50 μm slits drilled in a thin (0.125 mm) tantalum foil placed about 35 cm from the gun cathode. The location of the slits in the beam line was carefully chosen to allow for measurement of the emittance during the minimum of the emittance compensation process. In order to reconstruct the phase space, the beamlets are imaged downstream of the slits using a scintillating yttrium aluminum garnet (YAG) crystal and charge-coupled device (CCD) camera. By measuring the emittance at this location, it is desired to demonstrate the best quality electron beam that could be delivered to a booster linac for additional acceleration. Though this experiment does not currently employ the use of such a linac, it should be noted that the ability to maintain the minimum emittance value over the acceleration process will depend on careful choice of injection location, RF phase, and accelerating gradient. The beam energy in this experiment is determined with a 90° bend, Browne-Buechner style magnetic spectrometer. The spectrometer is imaging in the bend plane, resulting in a better than 1% energy resolution.

Beam simulations

The emittance compensation was designed to be effective for a 0.1 nC beam with energy of at least 2 MeV. The high energy is necessary to limit beam degradation due to space charge forces and velocity spread during transport. In this case, PARMELA simulations indicate that a normalized rms emittance of 0.5π mm mrad can be produced after emittance compensation (see Fig. 5). For lower energy beams ($\sim$1 MeV), the simulations showed that the emittance compensation is much less effective, with the normalized emittance for a 50 pC bunch increasing from about 1π mm mrad at the gun exit to about 3π mm mrad after transport to the slits. It is evident that the successful production of ultrahigh brightness beams in high frequency electron sources will depend on the attainability of the high field gradients necessary to produce a beam of sufficient energy. For a $1\frac{1}{2}$ cell gun, peak accelerating fields in excess of 300 MV/m will be required to obtain these parameters. Assuming that a 2 MeV beam can be produced, however, the normalized rms brightness of the beam defined by

$$B_n = \frac{2I}{\varepsilon_n^2}, \tag{4}$$

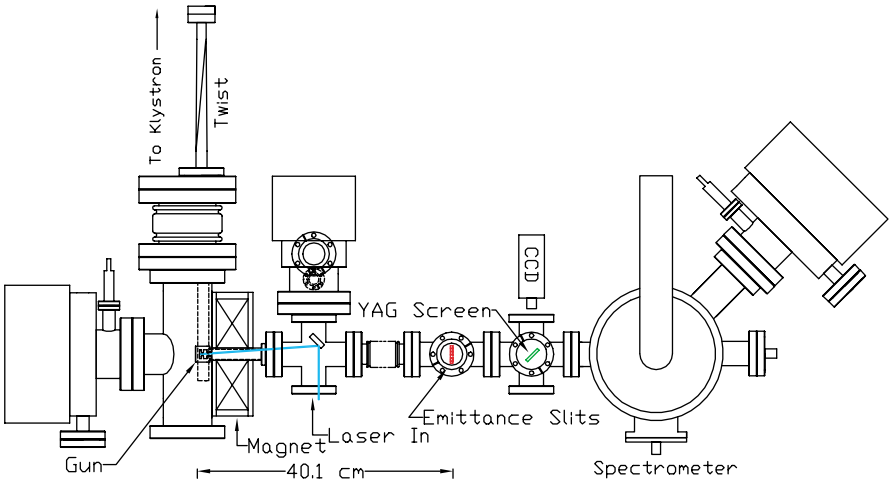

FIG. 4. (Color) Schematic of the RF gun beam line.

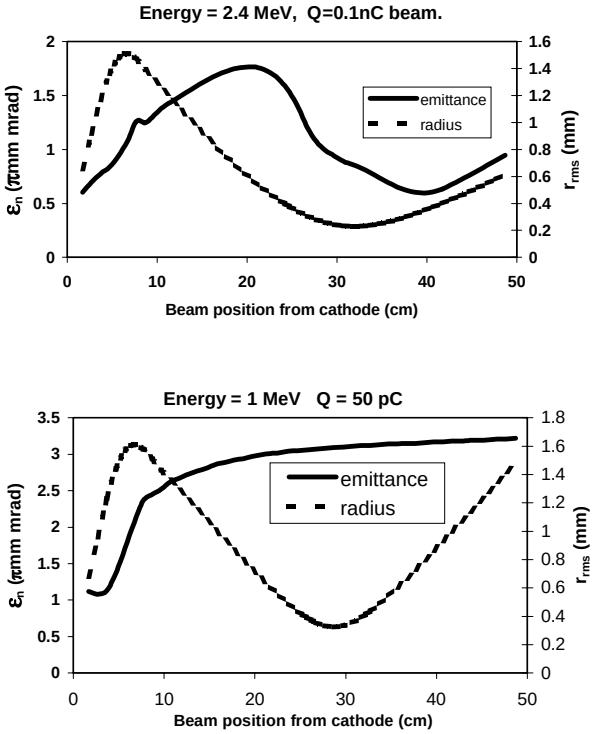

FIG. 5. PARMELA simulation of emittance compensation for a $1\frac{1}{2}$ cell gun for the case of a 2 MeV beam (top) and a 1 MeV beam (bottom). Emittance compensation is shown to be effective for the high energy case.

where ε_n is the normalized rms emittance and I is the peak current in the electron bunch, could reach values of about 800 $\mathrm{A}/(\pi\ \mathrm{mm\,mrad})^2$. This would represent a significant advance in electron beam sources, allowing for breakthroughs in accelerators designed for various application, including TeV colliders and free electron lasers.

IV. HIGH POWER OPERATION OF THE EXPERIMENT

The high power experiment utilizes a 17 GHz relativistic klystron amplifier constructed by Haimson Research Corporation (HRC) [9] to provide a 50 ns to 1 μs pulse of up to 26 MW of microwave power. The klystron is driven by a 560 kV, 1 μs flattop modulator pulse. A 0.27 μperv Thomson-CSF gun produces a space-charge limited electron beam at 560 kV with 95 A transmitted through the klystron. The amplifier chain includes a traveling wave tube (TWT) amplifier to provide up to 5 W to the klystron. The klystron gain is approximately 67 dB. To date, up to 4 MW of incident power have been coupled into the RF gun cavity yielding accelerating gradients approaching 200 MV/m.

A. Laser to RF phase stability

The laser beam for the RF gun photocathode is generated by a Ti:sapphire laser system, which produces 2 ps, 1.5 mJ pulses at 800 nm after chirped pulse amplification. The pulse duration of 2 ps was verified using a single-shot autocorrelator. These pulses are frequency tripled to 10–20 μJ of UV, and then focused on the back wall of the copper cavity. In order to ensure that the photoemission is successful in producing an electron beam on every shot, a sophisticated timing scheme is required to force the synchronization of the laser arrival time to the RF phase within the gun. The 84 MHz Ti:sapphire laser oscillator provides both the initial 2 ps, low energy, 800 nm laser pulse for input into a chirped pulse regenerative amplifier, as well as an initial low frequency RF signal (17 GHz/204 = 84 MHz) which is filtered and used as input into a phase locked 17 GHz yttrium iron garnet (YIG) oscillator. The YIG oscillator output is then used as the input into the TWT amplifier, which in turn is used as input to the klystron. Figure 6 shows a measurement of the phase stability obtained by observing the percentage of shots where an electron beam is detected with a Faraday cup as a function of RF phase shift. The width of this probability spectrum can be used to estimate the phase stability to be about $\pm 15°$. We are currently pursuing techniques for further reducing this jitter.

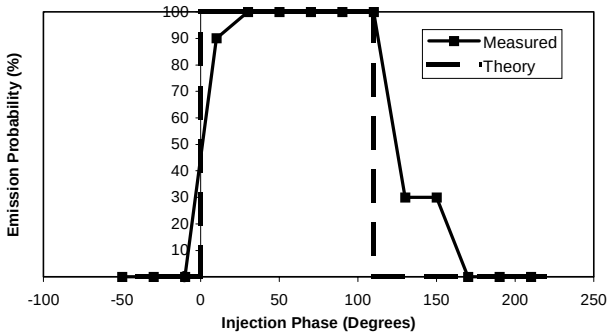

FIG. 6. Measured probability of laser induced electron emission from the RF gun as a function of RF phase shifter setting. Comparison to that predicted from theory suggests a phase stability of about $\pm 15°$ (or 2 ps).

B. Bunch charge and phase stability

The beam measurements performed on the new beam line have consisted of Faraday cup measurements of the beam bunch charge exiting the RF gun downstream of the laser injection chamber, transverse profile measurements with use of a YAG screen and CCD camera, and emittance measurements using a slit technique. With 15 μJ of UV incident on the gun cathode, and about 200 MV/m accelerating gradients in the half cell, bunch charges up to 0.11 nC have been observed. This corresponds to a quantum efficiency for the copper cathode of about 3×10^{-5}.

Field enhancement of the laser induced electron emission was observed by varying the laser injection phase. According to photoemission theory, the work function of a material will be reduced in the presence of an electric

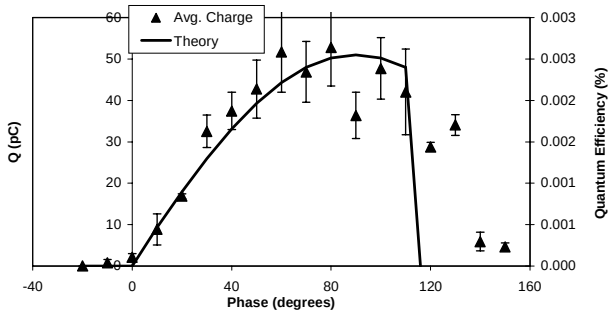

FIG. 7. Average charge versus laser injection phase demonstrating the Schottky effect. The average laser energy for this scan was about 10 μJ, corresponding to a peak quantum efficiency, η, of about 2.5×10^{-5}.

field E, such that there is an effective work function given by [10]

$$\Phi_{\text{eff}} = \Phi_0 - \sqrt{\frac{eE}{4\pi\varepsilon_0}}, \tag{5}$$

where Φ_0 is the cathode work function, E is the electric field at the cathode, e is the electron charge, and ε_0 is the permittivity of free space. The quantum efficiency goes as the square of the difference between the incident photon energy and the effective cathode work function, which leads to a predicted bunch charge versus RF injection phase dependence given by [10]

$$Q_b \propto \left(E_\nu - \Phi_0 + \sqrt{\frac{eE\sin(\varphi)}{4\pi\varepsilon_0}}\right)^2, \tag{6}$$

where Q_b is the beam bunch charge, φ is the laser injection phase, and E_ν is the photon energy. This scaling agrees well with the measured charge versus laser injection phase data shown in Fig. 7. The gradual fall off in charge for injection phases exceeding 100° is due primarily to injection phase jitter. The theoretical curve shows a falloff of about 10°, corresponding to the laser pulse width.

C. Beam imaging and emittance measurements

Transverse field profile measurements have been performed using a YAG crystal as a scintillator and storing the image using a CCD camera and frame grabber. The frame grabber was triggered with respect to the firing of the high voltage modulator in order to synchronize the acquired frame with the presence of the electron beam. Because of diffuse reflections of the laser light from the injection mirror and the gun cathode, it was necessary to filter out the wavelengths associated with the laser (i.e., 800, 400, and 266 nm). Figure 8 shows a typical transverse beam profile measurement for a beam near its waist after a soft focus at the position of the YAG screen (about 39 cm downstream of the emittance compensating solenoid). The profile is nearly Gaussian with an rms radius of about 0.6 mm. The beam energy was measured to be 0.9 MeV with the magnetic spectrometer. This agrees with the energy calculated based on a peak accelerating gradient of 170 MeV/m at the cathode. This field gradient is verified from calculations of the stored energy based on forward and reflected RF power measurements.

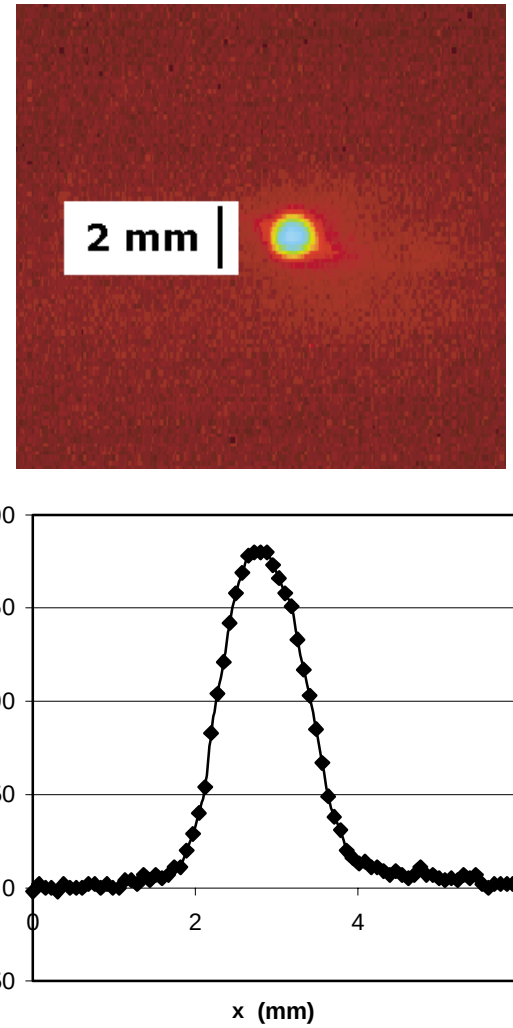

FIG. 8. (Color) Image of the 0.9 MeV electron beam (top) with Gaussian profile and 0.6 mm rms beam radius (bottom). The beam is imaged with a YAG crystal placed in the beam path.

Emittance measurements were performed using a multiple slit technique. This technique has the advantage of being a single shot measurement, as well as being suitable for space charge dominated beams. The ability to measure the emittance in a single shot is particularly important since the shot to shot emittance fluctuations resulting from the laser to RF phase jitter would make multiple shot methods, such as a quadrupole scan or a single slit method, extremely difficult. In the multiple slit measurement, individual beamlets are produced about 35 cm from the gun cathode by placing an array of 50 μm slits in the beam path. The slits were laser drilled into 125 μm tantalum foil, which is thick enough to sufficiently scatter out any transmitted electrons with energies up to 2 MeV. After passing through the slits, the beamlets travel through a drift space of about 13 cm before intersecting the YAG screen.

By measuring the width of each beamlet at the YAG screen position, as well as the relative intensity of each beamlet over the entire transverse dimension of the beam, the Twiss parameters can be determined and the geometric rms emittance can be calculated. This can be understood by examining the relationship between the phase space ellipse (see Fig. 9) and the Twiss parameters, given by

$$\gamma x^2 + 2\alpha x x' + \beta x'^2 = \varepsilon\,, \tag{7}$$

where ε is the geometric emittance and α, β, and γ are the Twiss parameters [11], and are correlated by the relation

$$\beta\gamma - \alpha^2 = 1\,. \tag{8}$$

The growth in the width of each beamlet during the transport from the slit to the screen provides a measurement of $\sqrt{\varepsilon/\beta}$, while the number and relative intensity of the beamlets coupled with the known spacing of the slits provides for a measurement of the rms beam size, or $\sqrt{\beta\varepsilon}$. The rms geometric emittance can be easily derived from these two measurements. For completeness, all three Twiss parameters can be determined by additionally finding the overall divergence of the beam between the slits and the screen, and using Eq. (8).

A typical emittance measurement can be see in Fig. 10. The bunch charge for each measurement is estimated by integrating over the intensity profile of the beamlets. A roughly linear dependence between emittance and charge is observed, which is in good agreement with theory [12] as well as with PARMELA simulations. Figure 11 shows the measured dependence of emittance on charge with that predicted by PARMELA simulations of the acceleration process in the gun and transport through the emittance compensating solenoid and drift space to the location of the slits. For these beam energies (0.8–1.0 MeV), the simulations suggest the emittance compensation is not effective, resulting in a roughly threefold space charge induced emittance growth between the exit of the gun and the location of the slits. While this results in a larger than ideal emittance, the beam quality produced from this gun is still quite high. For the measured normalized emittance of $\varepsilon_n \approx 3\,\pi$ mm mrad for a 50 pC beam at the location of the slits, an emittance of about $1\,\pi$ mm mrad at the exit of the RF gun can be inferred, corresponding to a normalized rms brightness of

$$B_n = \frac{2I}{\varepsilon_n^2} \approx 80\ \mathrm{A}/(\pi\ \mathrm{mm\,mrad})^2. \tag{9}$$

While this result is comparable to the best results produced from lower frequency RF guns, it falls short of representing a record high brightness beam, as can be seen from comparisons to the results obtained at both the Accelerator Test Facility (ATF) at Brookhaven and the Advanced Free Electron Laser (AFEL) at Los Alamos (see Fig. 12) [13,14]. It should also be stressed that the brightness value

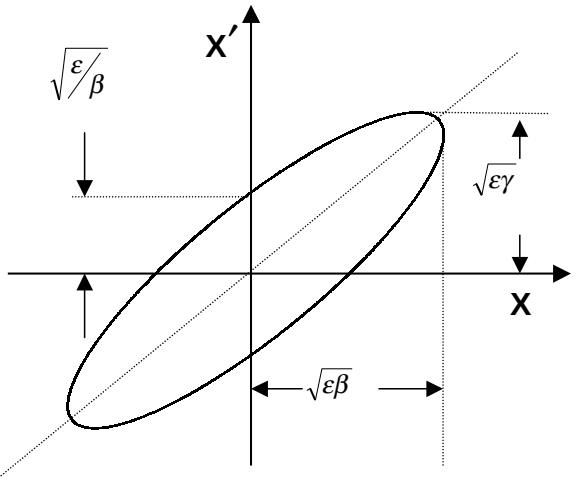

FIG. 9. Phase space ellipse. ε is the geometric emittance, while α, β, and γ are the Twiss parameters.

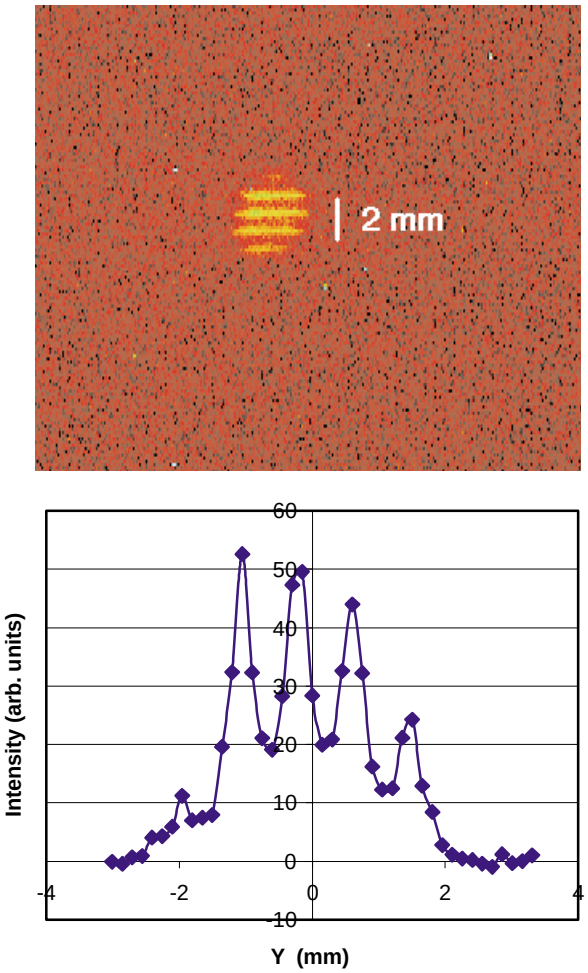

FIG. 10. (Color) Image of individual beamlets produced by the slits after a 13 cm drift length (top), and the relative intensity of the beamlets averaged over x as a function of y (bottom). The geometric emittance of this beam is $0.9\,\pi$ mm mrad with an estimated bunch charge of 12 pC. The relativistic factor $\beta\gamma$ is about 2.5.

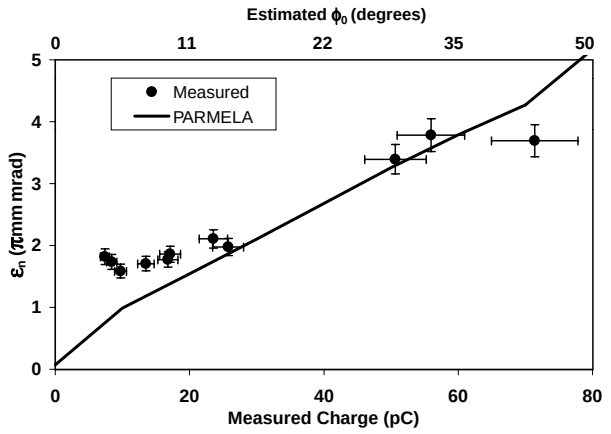

FIG. 11. Dependence of normalized emittance on charge for a 0.8 MeV beam as determined from measurement (dots) and PARMELA simulations (solid line). The incident UV laser energy is about 15 μJ. Estimates of the laser injection phase, ϕ_0, based on field enhancement of the quantum efficiency, are displayed on the upper horizontal axis.

expressed in Eq. (9) is dependent on the validity of the PARMELA simulations (Fig. 5) in describing the evolution of the measured emittance between the gun and the location of the emittance measurement. Additionally, since the emittance minimum, in this case, occurs very early in the beam transport, the ability to maintain this beam brightness will depend on the ability to place a booster linac within a few centimeters of the gun exit, which may be challenging in practice.

Currently, the RF gun is located adjacent to a 25 MeV 17 GHz accelerator, 0.5 m in length, constructed by Haimson Research Corporation. This accelerator is designed to allow either a conventional dc gun injector operating at an energy near 0.5 MeV, or an RF gun injector with a beam

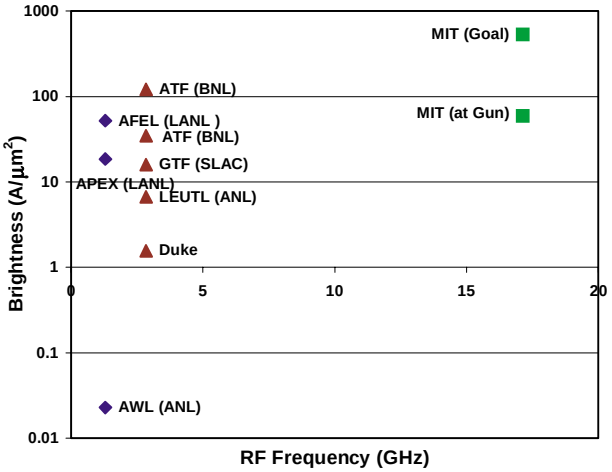

FIG. 12. (Color) Beam brightness for various RF photoinjectors. Both the beam brightness obtained with the 1.5 cell MIT gun as well as the goal of 800 A/(π mm mrad)^2 are displayed.

energy up to 2 MeV [15]. The dc gun injector has already been successfully tried with this accelerator. The beam from the present RF gun, which can in principle be placed quite close to the input of the accelerator, would also be suitable for injection into the HRC accelerator. In the near future, we plan to test the accelerator with an RF gun injector.

In order to produce the design brightness of about 800 A/(π mm mrad)^2, corresponding to $\varepsilon_n \approx 0.5\pi$ mm mrad for a 100 A peak current beam, the energy of the electron beam must be increased to at least 2 MeV. In this case, the space charge forces are greatly reduced, and the longitudinal integrity of the beam is not degraded by large velocity spreads, allowing the emittance compensation to be effective (Fig. 5). For the $1\frac{1}{2}$ cell gun, peak fields of over 300 MV/m must be obtained in order to reach this beam energy. However, RF breakdown in the gun has limited sustainable field gradients to about 200 MV/m, which has limited the obtainable beam energy to about 1 MeV. We are currently pursuing methods to overcome this problem, including the construction of an RF gun with additional cells to enable the production of a higher energy beam without the need for higher accelerating gradients.

V. CONCLUSIONS

A tunable 17 GHz RF gun was built and field profile measurements were performed by means of a "bead hang" method. The tunability of the new gun allowed for good field balance to be achieved between the half and the full cells. A new beam line and emittance compensating solenoid were also built for improved operation and diagnostics. High power conditioning of the gun has yielded accelerating gradients of 200 MV/m, and electron beam emissions of over 0.1 nC have been measured corresponding to a quantum efficiency of 3×10^{-5} for the copper cathode. Schottky enhancement of photoemission was verified, and laser to RF phase stability of 2 ps was measured. An rms normalized emittance of 3π mm mrad was measured after 35 cm of beam transport from the gun for a 1 MeV, 50 pC beam, in good agreement with simulations. The maximum beam energy produced by the $1\frac{1}{2}$ cell gun was limited to about 1 MeV by RF breakdown when the field gradient exceeds 200 MV/m. Efforts are underway to overcome this problem and produce a 2 MeV beam. If successful, a 100 pC, 1 ps electron bunch with a normalized emittance of 0.5π mm mrad should be obtainable after emittance compensation.

ACKNOWLEDGMENTS

This work is supported by the Department of Energy, Division of High Energy Physics. We would like to thank Dr. Jake Haimson and Haimson Research Corporation for extensive help and advice, Bill Mulligan, whose dedication

and expertise have been instrumental in the operation of the experiment, and Dr. Michael Shapiro and Dr. Chiping Chen for their helpful discussions on the theoretical aspects of the experiment.

[1] R. Carr, in *Synchrotron Radiation Instrumentation*, edited by E. Fontes, AIP Conf. Proc. No. 417 (AIP, New York, 1997), pp. 29–34.

[2] J. Rosenzweig and E. Colby, in *Proceedings of the 1995 Particle Accelerator Conference, Dallas* (IEEE, Piscataway, NJ, 1995), pp. 957–960.

[3] L. Lin, S. Chen, and J. Wurtele, in *Advanced Accelerator Concepts: Sixth Annual Conference*, edited by P. Schoessow, AIP Conf. Proc. No. 335 (AIP, New York, 1995), pp. 704–707.

[4] C. Ho, T. Yang, W. Lau, M. Horny, J. Hwang, M. Yeh, Y. Tsai, F. Hartmann, E. Landahl, H. Baldis, N. Luhmann, and A. Troha, in *Proceedings of the 1999 Particle Accelerator Conference, New York* (IEEE, Piscataway, NJ, 1999), Vol. 3, pp. 2000–2002.

[5] S. Trotz, W. Brown, B. Danly, J.-P. Hogge, M. Khusid, K. Kreischer, M. Shapiro, and R. Temkin, in *Advanced Accelerator Concepts: Seventh Workshop*, edited by S. Chattopadhyay, J. McCullough, and P. Dahl, AIP Conf. Proc. No. 398 (AIP, New York, 1996), pp. 717–729.

[6] D. Palmer, M. Hogan, M. Ferrario, and L. Serafini, in *Proceedings of the 1999 Particle Accelerator Conference, New York* (Ref. [4]), pp. 1997–1999.

[7] W. J. Brown, S. Trotz, K. E. Kreischer, M. Pedrozzi, M. A. Shapiro, and R. J. Temkin, Nucl. Instrum. Methods Phys. Res., Sect. A **425**, 441 (1999).

[8] S. Hanna, R. Loewen, H. Hoag, R. Miller, R. Ruth, and J. Wang, in *Proceedings of the 1997 Particle Accelerator Conference, Vancouver, Canada* (IEEE, Piscataway, NJ, 1998), Vol. 1, pp. 539–541.

[9] J. Haimson, B. Mecklenburg, and B. G. Danly, in *Pulsed RF Sources for Linear Colliders*, edited by R. C. Fernow, AIP Conf. Proc. No. 337 (AIP, New York, 1995), pp. 146–159.

[10] M. Cardona and L. Ley, *Photoemission in Solids* (Springer, New York, 1978), 2nd ed., p. 23.

[11] H. Wiedemann, *Particle Accelerator Physics* (Springer-Verlag, New York, 1993).

[12] K.-J. Kim, Nucl. Instrum. Methods Phys. Res., Sect. A **275**, 201 (1989).

[13] P. O'Shea, in *Proceedings of The 2nd ICFA Advanced Accelerator Workshop* (World Scientific, River Edge, NJ, 2000), pp. 17–26; http://stout.physics.ucla.edu/papers/ICFA99/osheaweb.pdf.

[14] D. Nguyen and V. Yakimenko, in *Proceedings of The 2nd ICFA Advanced Accelerator Workshop* (Ref. [13]), pp. 447–453.

[15] J. Haimson and B. Mecklenburg, in *Proceedings of the 1995 Particle Accelerator Conference, Dallas* (Ref. [2]), pp. 755-757.